Supporting Information

Magnetic Interaction Affecting the Zero-field Single-Molecule Magnet Behaviors in Isomorphic $\{Ni^{II}_2Dy^{III}_2\}$ and $\{Co^{II}_2Dy^{III}_2\}$ Tetranuclear Complexes

Haipeng Wu,[†,§] *Min Li,*[†,§] *Sheng Zhang,*[†,‡] *Hongshan Ke,*[†] *Yiquan Zhang,*[*,⊥] *Guilin Zhuang,*[*,‖] *Wenyuan Wang,*[†] *Qing Wei,*[†] *Gang Xie,*[†] *Sanping Chen*[*,†]

[†] Key Laboratory of Synthetic and Natural Functional Molecule Chemistry of Ministry of Education, College of Chemistry and Materials Science, Northwest University, Xi'an, 710127, China

[‡] College of Chemistry and Chemical Engineering, Baoji University of Arts and Sciences, Baoji, 721013, China

[⊥] Jiangsu Key Laboratory for NSLSCS, School of Physical Science and Technology, Nanjing Normal University, Nanjing 210023, China

[‖] College of Chemical Engineering, Zhejiang University of Technology, Hangzhou, 310032, China

[§] These authors contributed equally to this work.

*Corresponding authors

Dr. Yiquan Zhang

E-mail: zhangyiquan@njnu.edu.cn

Dr. Guilin Zhuang

E-mail: glzhuang@zjut.edu.cn

Dr. Sanping Chen

E-mail address: sanpingchen@126.com

Table of contents

Figure S15. Arrhenius plots for the relaxation times (τ) extracted from the frequency dependence of χ'' data for **4** in an external dc magnetic field of 800Oe.

Figure S16. Calculated complete structures of the Dy^{III} and Ni^{II} fragments of complex **1**; H atoms are omitted.

Figure S17. Orientations of the local main magnetic axes of the ground Kramers doublet on Dy^{III} of complexes **1** and **4**.

Table S4. Relaxation fitting parameters from Least-Squares Fitting of $\chi''(\omega)$ data for complex **4**.

Table S5. Relaxation fitting parameters from Least-Squares Fitting of $\chi''(\omega)$ data for complex **4**.

Figure S15. Calculated complete structures of the Dy^{III} and Ni^{II} fragments of complex **1**; H atoms are omitted.

Table S6. Calculated energy levels (cm^{-1}), $\boldsymbol{g}$ (g_x, g_y, g_z) tensors and m_J values of the lowest Kramers doublets (KDs) of the individual Dy^{III} fragment of complexes **1** and **4**.

Table S7. Calculated several lowest energy levels (cm^{-1}) and $\boldsymbol{g}$ tensors of the individual Co^{II} and Ni^{II} fragments of complexes **1** and **4**.

Figure S16. Orientations of the local main magnetic axes of the ground Kramers doublet on Dy^{III} of complexes **1** and **4**.

Table S8. Exchange energies (cm^{-1}) and main values of the g_z for the lowest eight exchange doublets of **1** and **4**.

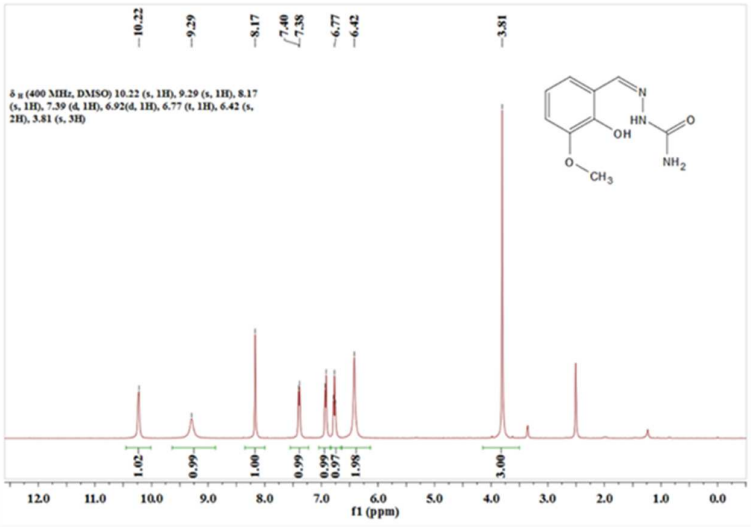

Figure S1. ^{1}H NMR of (2-hydroxy-3-methoxybenzylidene) semicarbazide (H_2hms).

Table S1. Crystal data and structure refinement summary for coordination complexes **1**-**6**.

	1	**2**	**3**	**4**	**5**	**6**
Empirical formula	$C_{32}H_{50}Dy_2N_8Ni_2O_{28}$	$C_{32}H_{50}Gd_2N_8Ni_2O_{28}$	$C_{32}H_{50}Y_2N_8Ni_2O_{28}$	$C_{32}H_{50}Dy_2N_8Co_2O_{28}$	$C_{32}H_{50}Gd_2N_8Co_2O_{28}$	$C_{32}H_{50}Y_2N_8Co_2O_{28}$
Formula weight	1437.22	1426.72	1290.04	1437.66	1427.16	1290.48
Crystal system	Monoclinic	Monoclinic	Monoclinic	Monoclinic	Monoclinic	Monoclinic
Space group	P2(1)/c	P2(1)/c	P2(1)/c	P2(1)/c	P2(1)/c	P2(1)/c
a (Å)	10.4080(19)	10.4266(14)	10.451(2)	10.4508(12)	10.4667(14)	10.441(2)
b (Å)	19.364(4)	19.390(3)	19.411(4)	19.368(2)	19.404(3)	19.362(4)
c (Å)	12.748(2)	12.7481(16)	12.757(3)	12.7458(14)	12.8071(17)	12.742(3)
α (°)	90	90	90	90	90	90
β (°)	111.793(3)	111.871(2)	111.809(4)	111.561(2)	111.586(2)	111.583(4)
γ(°)	90	90	90	90	90	90
V (Å^3)	2385.5(7)	2391.8(5)	2402.7(8)	2399.4(5)	2418.7(6)	2395.2(9)
Z	2	2	2	2	2	2
D_c (g m^{-3})	2.001	1.981	1.783	1.990	1.960	1.789
μ (mm^{-1})	3.975	3.613	3.263	3.858	3.480	3.180
F (000)	1420	1412	1312	1416	1408	1308
Reflns collected/unique	10895 / 3800	11802 / 4209	12776 / 4703	11773 / 4219	13676 / 5257	13073 / 4854
R_{int}	0.0794	0.0272	0.0572	0.0350	0.0219	0.0773
GOF on F^2	1.076	0.995	0.990	1.011	0.971	0.994
R_1[a] [$I > 2\sigma(I)$]	0.0738	0.0249	0.0408	0.0286	0.0225	0.0490
wR_2[b] (all data)	0.1976	0.0790	0.0819	0.0847	0.0624	0.0881
CCDC	1506841	1506842	1506844	1506837	1506838	1506840

[a] $R_1 = \Sigma(||F_o| - |F_c||)/\Sigma|F_o|$. [b] $wR_2 = [\Sigma w(F_o^2 - F_c^2)^2/\Sigma w(F_o^2)^2]^{1/2}$.

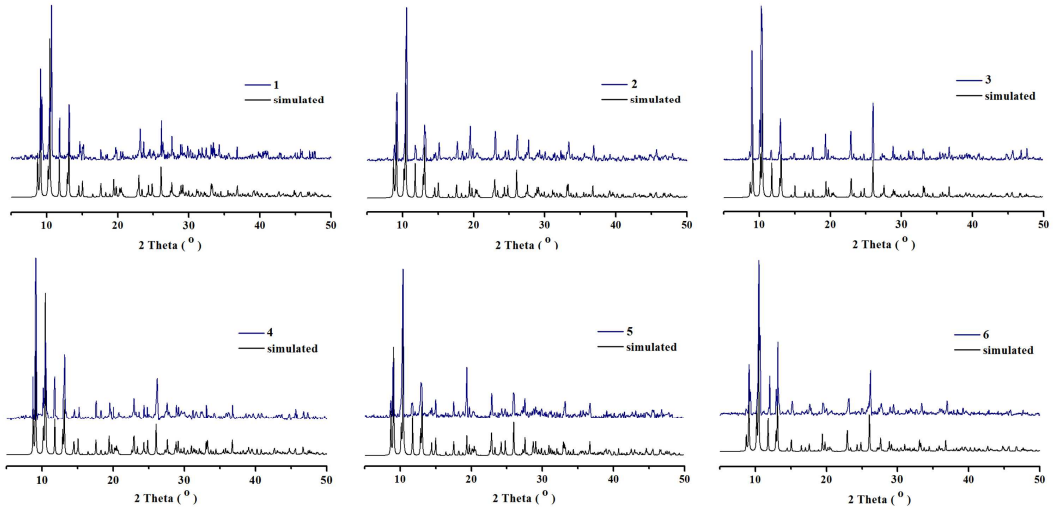

Figure S2. PXRD curves for **1-6**.

Table S2. Shape analysis for the metal centers of **1.**

ML9	JTC-9	JCCU-9	CCU-9	JCSAPR-9	CSAPR-9	JTCTPR-9	TCTPR-9
Dy1	14.961	9.766	8.715	2.848	**1.715**	3.440	4.145

JTC-9 (C_{3v}): Johnson triangular cupola J3
JCCU-9 (C_{4v}): Capped cube J8
CCU-9 (C_{4v}): Spherical-relaxed Capped cube
JCSAPR-9 (C_{4v}): Capped square antiprism J10
CSAPR-9 (C_{4v}): Spherical capped square antiprism
JTCTPR-9 (D_{3h}): Tricapped trigonal prism J51
TCTPR-9 (D_{3h}): Spherical tricapped trigonal prism

Table S3. Selected bond lengths (Å) and bond angles (o) for **1**.

Complex **1**								
Dy1		O2	2.270(6)	Dy1		C13	2.893(11)
Dy1		O7[1]	2.313(7)	Dy1		Ni1	3.4151(14)
Dy1		O5	2.330(7)	Dy1		Dy1[1]	3.9292(12)
Dy1		O8	2.340(6)	Ni1		N2	2.004(9)
Dy1		O10	2.411(7)	Ni1		O4	2.020(7)
Dy1		O7	2.485(7)	Ni1		O2	2.022(6)
Dy1		O9	2.504(7)	Ni1		O3	2.047(7)
Dy1		O1	2.542(8)	Ni1		O9	2.096(7)
Dy1		O6	2.566(7)	Ni1		O11	2.168(7)
O2	Dy1	O7[1]	141.2(2)	O10	Dy1	O9	143.2(2)
O2	Dy1	O5	74.5(2)	O7	Dy1	O9	71.1(2)
O7[1]	Dy1	O5	75.0(2)	O2	Dy1	O1	64.6(2)
O2	Dy1	O8	143.2(2)	O7[1]	Dy1	O1	153.0(2)

O7[1]	Dy1	O8	75.5(2)	O5	Dy1	O1	116.9(3)
O5	Dy1	O8	129.1(2)	O8	Dy1	O1	78.8(2)
O2	Dy1	O10	98.9(2)	O10	Dy1	O1	70.7(3)
O7[1]	Dy1	O10	93.0(2)	O7	Dy1	O1	107.7(2)
O5	Dy1	O10	70.7(2)	O9	Dy1	O1	129.2(2)
O8	Dy1	O10	70.5(2)	O2	Dy1	O6	71.7(2)
O2	Dy1	O7	118.1(2)	O7[1]	Dy1	O6	118.6(2)
O7[1]	Dy1	O7	70.1(3)	O5	Dy1	O6	136.7(2)
O5	Dy1	O7	134.1(2)	O8	Dy1	O6	94.0(2)
O8	Dy1	O7	68.8(2)	O10	Dy1	O6	140.6(3)
O10	Dy1	O7	138.6(2)	O7	Dy1	O6	50.4(2)
O2	Dy1	O9	71.8(2)	O9	Dy1	O6	71.8(2)
O7[1]	Dy1	O9	76.6(2)	O1	Dy1	O6	70.8(2)
O5	Dy1	O9	72.5(2)	N2	Ni1	O4	94.7(3)
O8	Dy1	O9	136.9(2)	N2	Ni1	O2	89.5(3)
O3	Ni1	O9	106.3(3)	O4	Ni1	O2	91.2(3)
N2	Ni1	O11	88.2(3)	N2	Ni1	O3	78.4(3)
O4	Ni1	O11	177.1(3)	O4	Ni1	O3	89.0(3)
O2	Ni1	O11	89.3(3)	O2	Ni1	O3	167.8(3)
O3	Ni1	O11	91.0(3)	N2	Ni1	O9	172.0(3)
O9	Ni1	O11	85.4(3)	O4	Ni1	O9	91.8(3)
O2	Ni1	O9	85.9(3)				

[1]1-X,-Y,1-Z

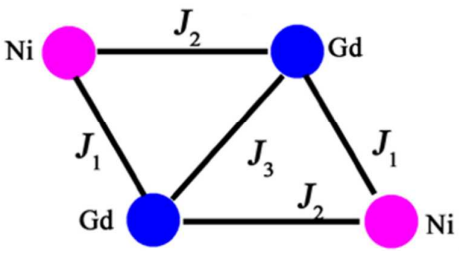

Figure S3. The connection Sketch of $\{Ni_2^{II}Gd_2^{III}\}$.

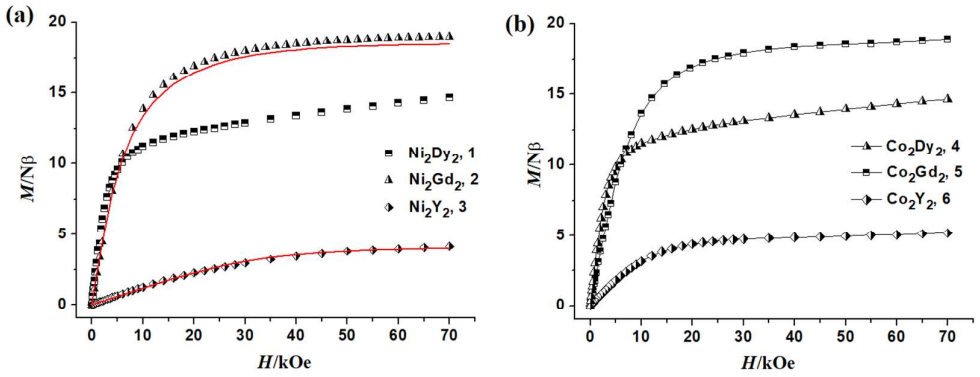

Figure S4. Field dependent magnetizations from 0 to 70 kOe at 2 K for complexes **1-3** (a) and **4-6** (b) (red solid lines represent the best simulation for **2** and **3**).

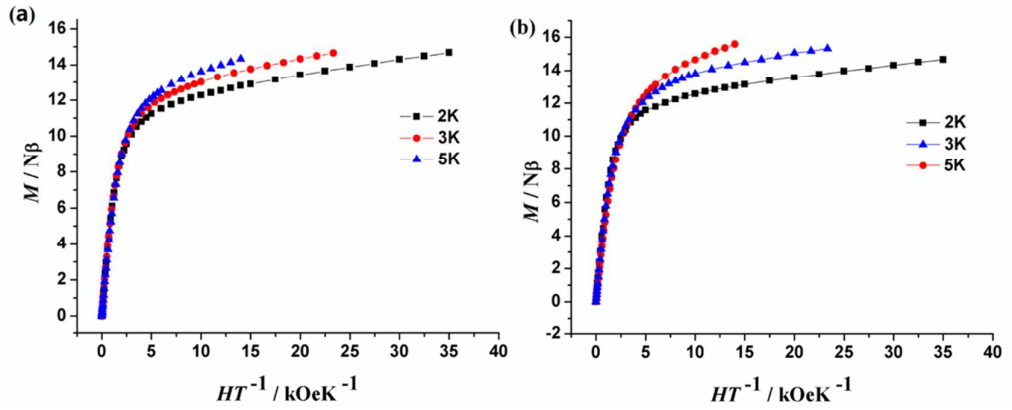

Figure S5. Field dependence of magnetizations of **1** (a) and **4** (b) at different temperatures below 5 K.

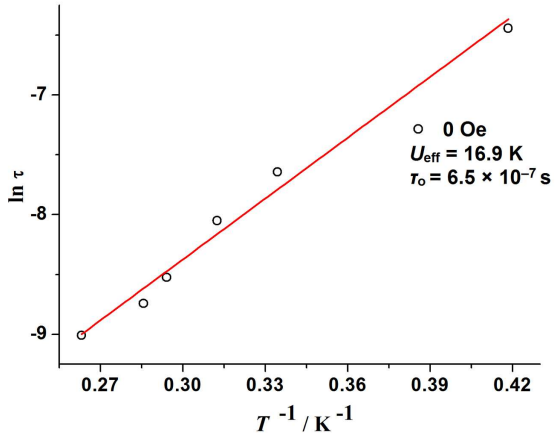

Figure S6 Relaxation time of the magnetization for **1** extracted from the temperature-dependent data for **1** under zero dc field. The red solid lines represent the fitting by the Arrhenius law.

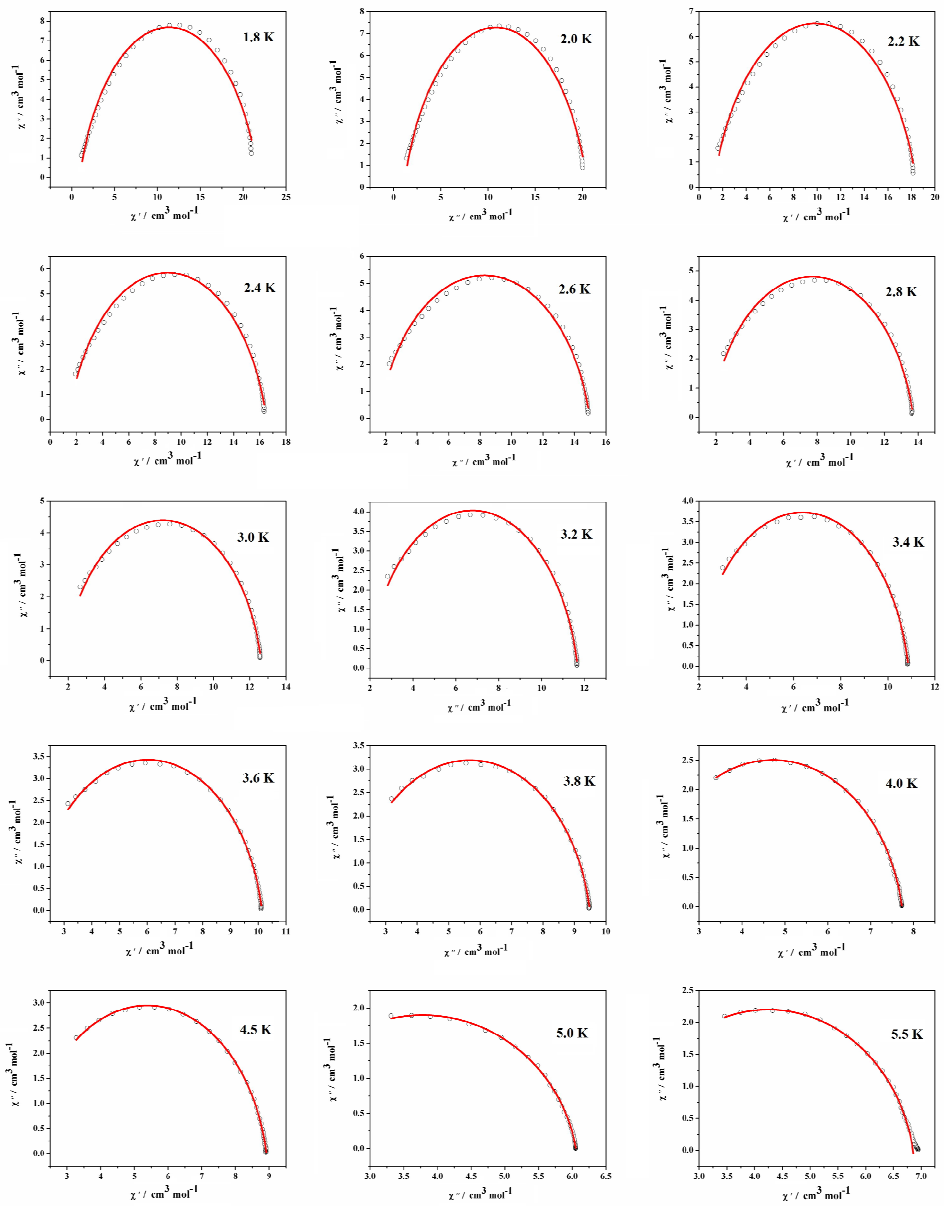

Figure S7 Simulations of dynamical susceptibility χ(ω) ranging from 1.8 to 5.5 K in a Cole-Cole diagram for complex **1**. Red lines were performed using the sum of two modified Debye functions with the fitting parameters in Table S3.

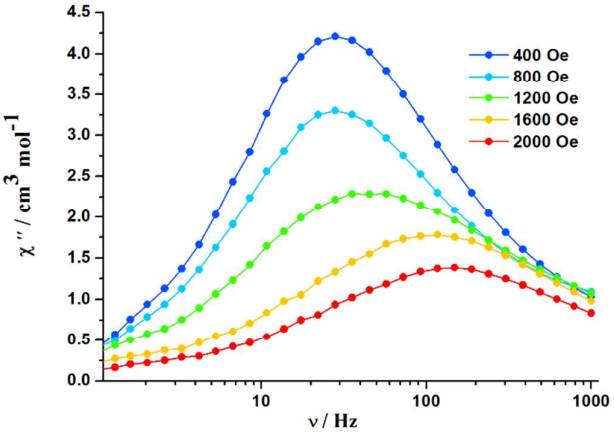

Figure S8 Field dependence of the out-of-phase signal *vs* frequency at 2 K for **1**.

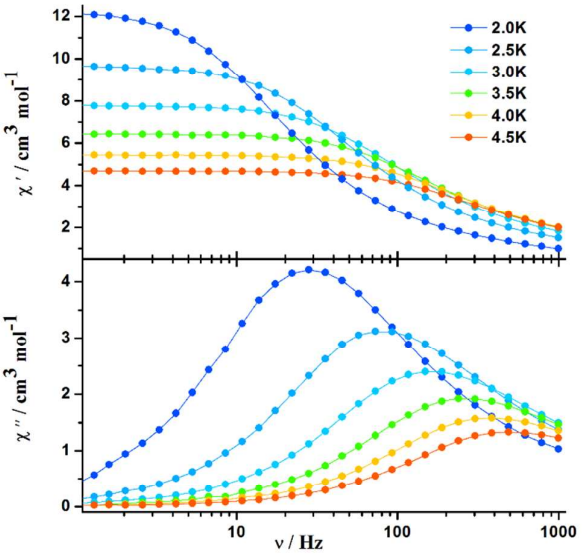

Figure S9 Frequency dependence of the in-phase χ' (top) and out-of phase χ'' (bottom) ac susceptibility signals for **1** under 400 Oe dc applied field.

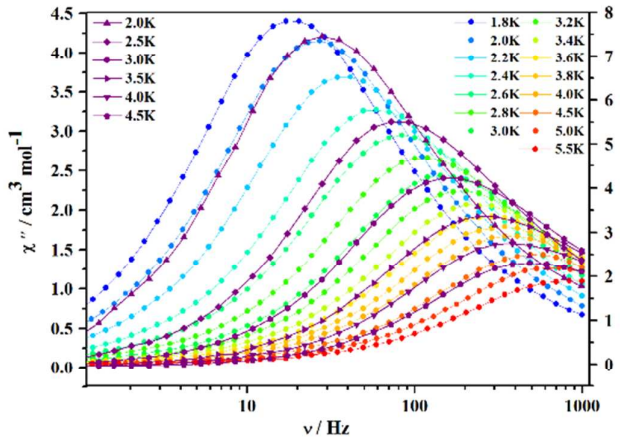

Figure S10 Comparison of the AC susceptibility data of χ'' vs. ν plot for **1** under a zero (multicolour circles) and applied dc field of 400 Oe (violet points).

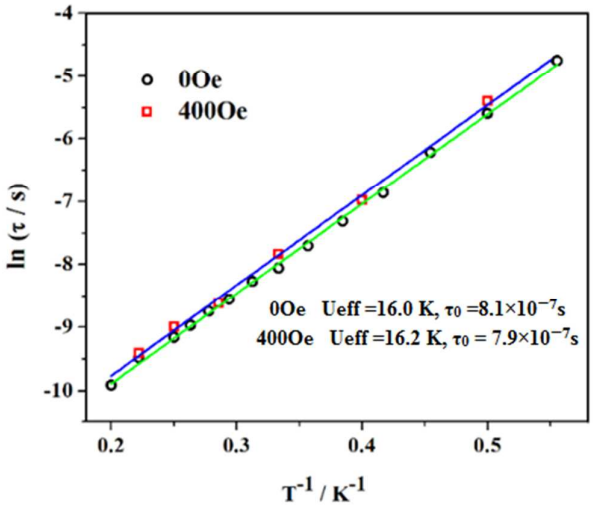

Figure S11 Arrhenius plots for the relaxation times (τ) extracted from the frequency dependence of χ'' data for **1** in an external dc magnetic field of 400Oe.

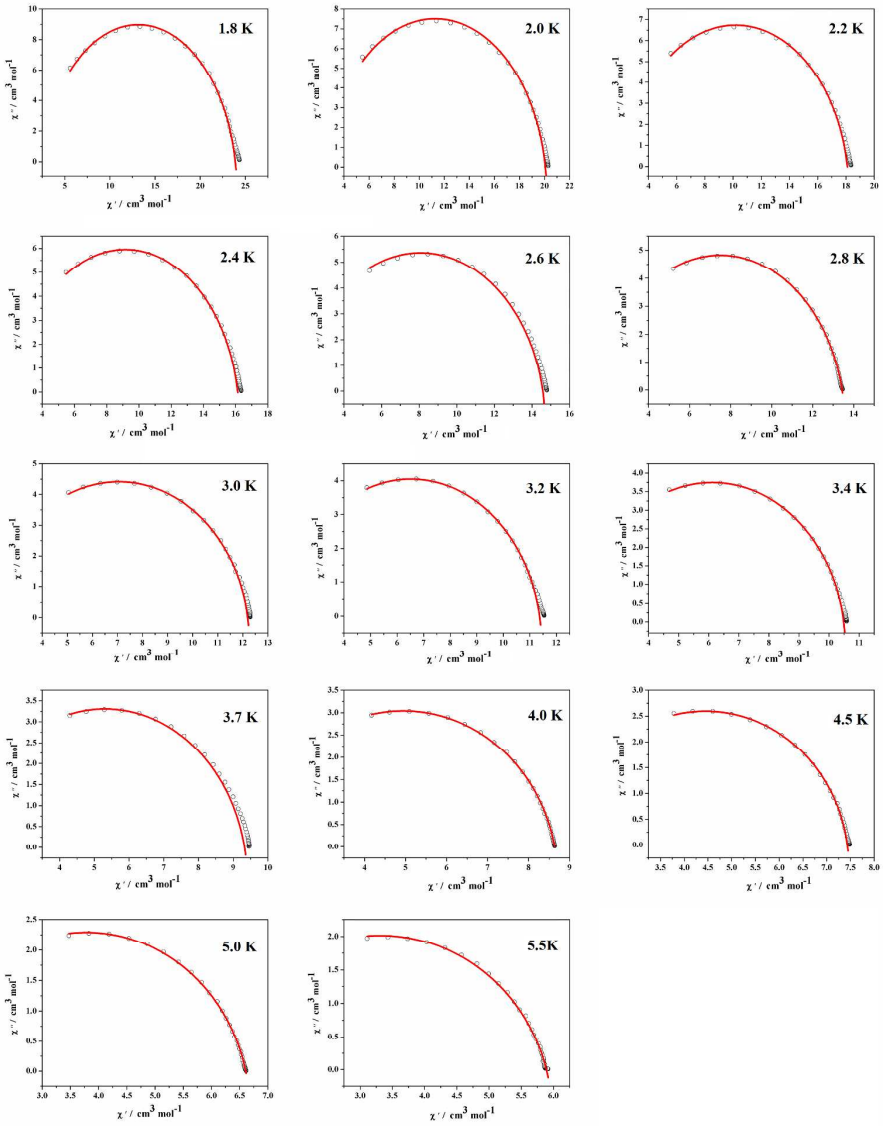

Figure S12 Simulations of dynamical susceptibility χ(ω) ranging from 1.8 to 5.5 K in a Cole-Cole diagram for complex **4**. Red lines were performed using the sum of two modified Debye functions with the fitting parameters in Table S4.

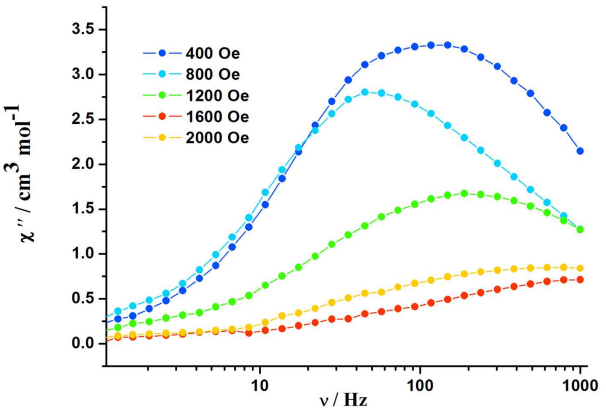

Figure S13 Field dependence of the out-of-phase signal *vs* frequency at 2 K for **4**.

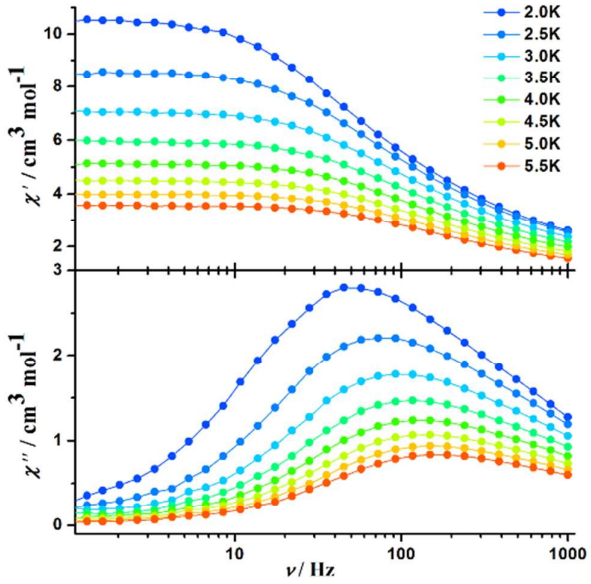

Figure S14 Frequency dependence of the in-phase χ' (top) and out-of phase χ'' (bottom) ac susceptibility signals for **4** under 800 Oe dc applied field.

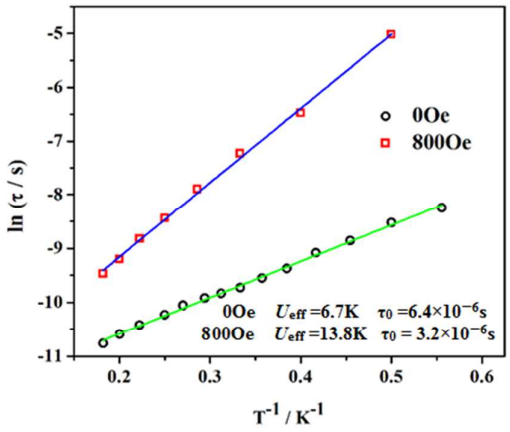

Figure S15 Arrhenius plots for the relaxation times (τ) extracted from the frequency dependence of χ'' data for **4** in an external dc magnetic field of 800Oe.

Table S4. Relaxation fitting parameters from Least-Squares Fitting of $\chi(\omega)$ data for complex **1**.

T (K)	$\Delta\chi_1$ (cm^3mol^{-1})	$\Delta\chi_2$ (cm^3mol^{-1})	α_1
1.8	21.7609	0.92888	0.19004
2.0	20.55478	1.07592	0.18302
2.2	18.47527	1.207	0.1755
2.4	16.51076	1.40864	0.16125
2.5	14.98212	1.57561	0.14918
2.8	13.7127	1.68623	0.14175
3.0	12.62687	1.76494	0.13344
3.2	11.68921	1.84053	0.12544
3.4	10.86506	1.89009	0.11782
3.6	10.13138	1.89065	0.11584
3.8	9.48697	1.85931	0.11282
4.0	8.91467	1.84621	0.11121
4.5	7.73074	1.70517	0.11645
5.0	6.85283	1.64232	0.10703
5.5	6.05501	1.50659	0.11399

Table S5. Relaxation fitting parameters from Least-Squares Fitting of $\chi(\omega)$ data for complex **4**.

T (K)	$\Delta\chi_1$ (cm^3mol^{-1})	$\Delta\chi_2$ (cm^3mol^{-1})	α_1
1.8	23.89679	2.3816	0.11455
2.0	20.06933	2.4903	0.09965
2.2	18.09983	2.25245	0.10296
2.4	16.12581	2.18425	0.10042
2.5	14.57764	1.55985	0.12249

2.8	13.43715	1.55895	0.13106
3.0	12.19592	1.90688	0.09693
3.2	11.36889	1.68194	0.11359
3.4	10.48858	1.75086	0.09748
3.7	9.33133	1.28409	0.12413
4.0	8.63724	1.25045	0.12314
4.5	7.43631	1.45751	0.08956
5.0	6.6068	0.95512	0.13227
5.5	5.88988	0.72919	0.15585

Ab initio calculation on individual lanthanide fragment

For the symmetric structures of complexes **1** and **4**, we only need to calculate one type of Dy^{III} and one transition metal center (Ni^{II} for **1** and Co^{II} for **4**) fragments for each of them. Complete-active-space self-consistent field (CASSCF) calculations on the individual Dy^{III} and transition metal fragments (see Figure S15 for the complete structure of complex **1**) of complexes **1** and **4** on the basis of X-ray determined geometry have been carried out with MOLCAS 8.0 program package[1]. In the calculation of Dy^{III} fragment, we replaced two Co^{II} or Ni^{II} ions with diamagnetic Zn^{II} ions, while in the calculation of Co^{II} or Ni^{II} fragment, we replaced the other transition metal and Dy^{III} ions with the diamagnetic Zn^{II} and Lu^{III} ions, respectively. For CASSCF calculations, the basis sets for all atoms are atomic natural orbitals from the MOLCAS ANO-RCC library: ANO-RCC-VTZP for Dy^{III}, Ni^{II} or Co^{II}; VTZ for close O and N; VDZ for distant atoms. The calculations employed the second order Douglas-Kroll-Hess Hamiltonian, where scalar relativistic contractions were taken into account in the basis set and the spin-orbit coupling was handled separately in the restricted active space state interaction (RASSI-SO) procedure. In the calculation of Dy^{III} fragment, the active electrons in 7 active spaces include all *f* electrons (CAS (9 in 7)) for complexes **1** and **4**, while in the calculation of transition metal fragment, the active electrons in 5 active spaces include all *d* electrons (CAS (7 in 5) for Co^{II} and CAS (8 in 5) for Ni^{II}) in the CASSCF calculation. To exclude all the doubts we calculated all the roots in the active space. We have mixed the maximum number of spin-free state which was possible with our hardware (all from 21 sextets, 128 from 224 quadruplets and 130 from 490 doublets for Dy^{III} fragments; all from 10 quadruplets, all from 40 doublets for Co^{II} fragment; all from 10 triplets, all from 15 singlets for Ni^{II} fragment).

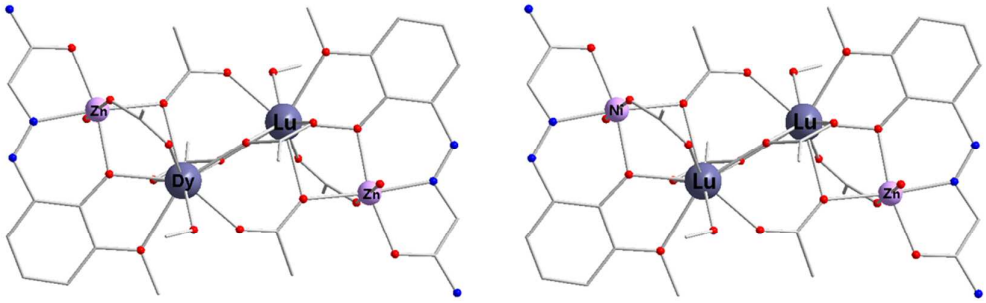

Dy^{III} fragment Ni^{II} fragment

Figure S16. Calculated complete structures of the Dy^{III} and Ni^{II} fragments of complex **1**; H atoms are omitted.

Table S6. Calculated energy levels (cm^{-1}), $\boldsymbol{g}$ (g_x, g_y, g_z) tensors and m_J values of the lowest Kramers doublets (KDs) of the individual Dy^{III} fragment of complexes **1** and **4**.

KDs	**1**			**4**		
	E/cm^{-1}	$\boldsymbol{g}$	m_J	E/cm^{-1}	$\boldsymbol{g}$	m_J
1	0.0	0.030 0.058 19.390	±15/2	0.0	0.039 0.080 19.342	±15/2
2	113.8	0.298 0.406 16.108	±13/2	103.1	0.346 0.477 15.989	±13/2
3	221.0	1.932 2.599 12.163	±11/2	206.2	2.492 3.961 10.953	±11/2
4	286.8	8.778 5.380 1.293	±7/2	264.1	8.015 6.388 1.125	±5/2
5	362.8	3.957 4.740 9.131	±1/2	332.5	2.633 3.581 10.236	±7/2
6	427.3	0.841 1.451 13.575	±9/2	396.7	0.756 1.193 13.616	±1/2
7	486.9	0.126 0.192 16.605	±5/2	445.9	0.161 0.214 16.857	±9/2
8	576.2	0.029 0.063	±3/2	505.2	0.033 0.060	±3/2

19.595	19.538

Table S7. Calculated several lowest energy levels (cm^{-1}) and ***g*** tensors of the individual Co^{II} and Ni^{II} fragments of complexes **1** and **4**.

1		**4**	
E/cm^{-1}	***g***	E/cm^{-1}	***g***
	2.323		5.586
0.0	2.311	0.0	4.672
	2.279		2.256
4.6		132.1	
7.3		908.3	

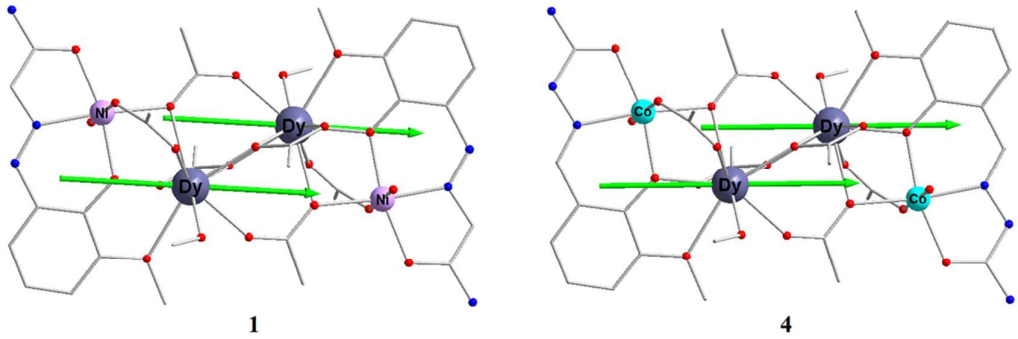

1 **4**

Figure S17. Orientations of the local main magnetic axes of the ground Kramers doublet on Dy^{III} of complexes **1** and **4**.

Fitting the exchange interaction in two complexes using Lines model based on CASSCF results

To fit the exchange interactions in two complexes, we took two steps to obtain them. Firstly, we calculated the mononuclear fragments using CASSCF to obtain the corresponding magnetic properties (see the first part). Then, the exchange interaction between the magnetic centers is considered within the Lines model[2], while the account of the dipole-dipole magnetic coupling is treated exactly. The Lines model is effective and has been successfully used widely in the research field of binuclear lanthanide single-molecule magnets.[3]

For complexes **1**–**2**, the exchange Hamiltonian is:

$$\hat{H}_{exch} = -J^{total}_{Dy1-Dy2}\hat{\tilde{S}}_{Dy1}\hat{\tilde{S}}_{Dy2} - J^{total}_{Dy1-Co1}(\hat{\tilde{S}}_{Dy1}\hat{\tilde{S}}_{Co1} + \hat{\tilde{S}}_{Dy2}\hat{\tilde{S}}_{Co2}) - J^{total}_{Dy1-Co2}(\hat{\tilde{S}}_{Dy1}\hat{\tilde{S}}_{Co2} + \hat{\tilde{S}}_{Dy2}\hat{\tilde{S}}_{Co1}) \quad (1)$$

$$\hat{H}_{exch} = -J^{total}_{Dy1-Dy2}\hat{\tilde{S}}_{Dy1}\hat{\tilde{S}}_{Dy2} - J^{total}_{Dy1-Ni1}(\hat{\tilde{S}}_{Dy1}\hat{\tilde{S}}_{Ni1} + \hat{\tilde{S}}_{Dy2}\hat{\tilde{S}}_{Ni2}) - J^{total}_{Dy1-Ni2}(\hat{\tilde{S}}_{Dy1}\hat{\tilde{S}}_{Ni2} + \hat{\tilde{S}}_{Dy2}\hat{\tilde{S}}_{Ni1}) \quad (2)$$

The $J^{total}_{Dy1-Dy2}$, $J^{total}_{Dy1-Co1}$, $J^{total}_{Dy1-Co2}$, $J^{total}_{Dy1-Ni1}$ and $J^{total}_{Dy1-Ni2}$ are parameters of the total magnetic interaction ($J^{total} = J^{diploar} + J^{exchange}$) between Dy1-Dy2, Dy1-Co1, Dy1-Co2, Dy1-Ni1 and Dy1-Ni2, respectively. The $\hat{\tilde{S}} = \pm 1/2$ is the ground pseudospin on the Dy^{III} and Co^{II} sites, while the spins on Ni^{II} sites are ±1, respectively. The dipolar magnetic coupling can be calculated exactly, while the exchange coupling constants were fitted through comparison of the computed and measured magnetic susceptibilities using the POLY_ANISO program.[4]

Table S8. Exchange energies (cm^{-1}) and main values of the g_z for the lowest exchange doublets of **1** and **4**.

	1		**4**	
	E	g_z	*E*	g_z
1	0.000	41.214	0.000	42.985
2	2.053	0.000	0.623	38.711
3	4.750	39.044	0.624	38.709
4	4.750	39.044	1.247	36.044
5	6.679	0.007	2.047	0.000
6	6.679	0.007	2.573	0.000
7	7.400	39.743	2.574	0.000
8	7.401	39.743	3.100	0.000
9	9.365	0.000		
10	9.365	0.000		
11	9.500	36.875		
12	11.305	0.000		
13	12.151	37.569		
14	12.151	37.569		
15	13.991	0.000		
16	13.991	0.000		

17	14.801	38.298		
18	16.677	0.000		

Reference

(1) Karlström, G.; Lindh, R.; Malmqvist, P. -Å.; Roos, B. O.; Ryde, U.; Veryazov, V.; Widmark, P. -O.; Cossi, M.; Schimmelpfennig, B.; Neograd y, P.; Seijo, L. MOLCAS: a Program Package for Computational Chemistry. *Comput. Mater. Sci*. **2003**, *28*, 222.

(2) Lines, M. E. *J. Chem. Phys*. **1971**, *55*, 2977.

(3) (a) Mondal, K. C.; Sundt, A.; Lan, Y. H.; Kostakis, G. E.; Waldmann, O.; Ungur, L.; Chibotaru, L. F.; Anson, C. E.; Powell, A. K. *Angew. Chem. Int. Ed*. **2012**, *51*, 7550. (b) Langley, S. K.; Wielechowski, D. P.; Vieru, V.; Chilton, N. F.; Moubaraki, B.; Abrahams, B. F.; Chibotaru, L. F.; Murray, K. S. *Angew. Chem. Int. Ed*. **2013**, *52*, 12014.

(4) (a) Chibotaru, L. F.; Ungur, L.; Soncini, A. *Angew. Chem. Int. Ed.*, **2008**, *47*, 4126. (b) Ungur, L.; Van den Heuvel, W.; Chibotaru, L. F. *New J. Chem.*, **2009**, *33*, 1224. (c) Chibotaru, L. F.; Ungur, L.; Aronica, C.; Elmoll, H.; Pilet, G.; Luneau, D. *J. Am. Chem. Soc.*, **2008**, *130*, 12445.